Photochemically Induced Silicon−Carbon Bond Cleavage in a Dimethylsilyl-Bridged Dicyclopentadienyl Diruthenium Complex

Thomas Fox[a] and Peter Burger*[a]

Keywords: Cyclopentadienes / Ruthenium / IR spectroscopy / Photochemistry / Rearrangements / Thermodynamics / Density functional calculations

The synthesis and X-ray crystal structure of the novel permethylated dimethylsilyl-bridged diruthenium complex $Me_2Si[(C_5Me_4)Ru(CO)_2]_2$ **(1)** is reported. The molecular structure displays a metal–metal bond of 2.7121(4) Å, which is supported by two symmetrical μ-bridging CO groups and, in addition, two terminal carbonyl ligands. In solution, exchange of these carbonyl groups is observed, as shown by ^{13}C NMR EXSY and VT IR-measurements. It is suggested that the exchange process proceeds via the energetically disfavoured intermediate **1a**, which displays four terminal CO ligands. This view is supported by density functional calculations, which indicate a C_2-symmetrical structure for **1a**. Photochemically induced cleavage of the silicon–carbon and Ru–Ru bonds in **1** results in complex **3**, which is thermodynamically uphill from **1** according to our DFT calculations. The molecular structure of complex **3** was unambiguously confirmed by X-ray crystallography.

Introduction

Thermal or photochemical skeletal rearrangements of dicyclopentadienyl ligands in dinuclear complexes with bridging cyclopentadienyl groups have recently received significant attention.[1−5] Perhaps the most exciting result in this area is the fulvalenediyl diruthenium system recently reported by Vollhardt and co-workers.[5] These complexes undergo photochemically induced C−C bond cleavage to give *energetically less-stable* products. Since this process can be thermally reversed, it has been anticipated that these systems might be potential light energy storage systems. As part of our research into oxidation catalysis, we have considered dicyclopentadienyl-bridged ditungsten complexes with metal−metal multiple bonds.[6] Recently, we have extended our research program to include the group 8 transition metals ruthenium and osmium. In the course of these studies, we observed facile, and quantitative, photochemically induced Si−C bond cleavage in the dimethylsilyl-bridged permethylated complex $Me_2Si[(C_5Me_4)Ru(CO)_2]_2$ (**1**). While this work was in progress, Bitterwolf et al. reported similar results in the parent complex $Me_2Si[(C_5H_4)Ru(CO)_2]_2$ (**2**),[7] which was shortly followed by an alternative synthesis for **2** and a short discussion on fluxionality in the parent compound by Zhou and coworkers.[8] In this paper, we will focus on kinetic and thermodynamic aspects of the fluxional processes in the metal−metal bonded complex **1** and its photochemical Si−C bond cleavage product **3**.'

Results and Discussion

In analogy to the parent complex **2** and the methano-bridged congener $CH_2[(C_5Me_4)Ru(CO)_2]_2$ (**4**), the dinuclear complex **1** was obtained from the treatment of the permethylated dimethylsilyl-bridged ligand with 0.66 equiv. $Ru_3(CO)_{12}$ in refluxing octane [Equation (1)].[8,9]

When the reaction according to Equation (1) was carried out under rigorously oxygen-free conditions, the ^1H NMR spectrum of the crude reaction mixture displayed, along with the signals of the major product **1**, additional peaks for a C_{2v} symmetrical minor product. The most prominent resonance of the minor product was a singlet at $\delta = -10.0$ in [D$_6$]benzene, indicative of a ruthenium hydride complex. In analogy with the hydride resonance in the unbridged pentamethyl cyclopentadienyl (Cp*) compound Cp*Ru(CO)$_2$H, which displays a singlet for the Ru hydride at $\delta = -10$,[10] we tentatively assigned these resonances to the presumed initial dihydride product $SiMe_2[(C_5Me_4)Ru(CO)_2H]_2$ (**5**). Complex **5** could then convert into the final product **1** with concomitant H_2 loss. Attempts to isolate the presumed dihydride complex **5**, either exclusively or as a major product, failed. We therefore carried out the reaction with few measures to exclude O_2 (see Experimental Section for details).[11]

Initial attempts to isolate the dinuclear product **1** from the reaction mixture by chromatography proved to be cumbersome, since, on alumina (Al_2O_3, neutral, act II−III), partial decomposition to give $[(C_5Me_4H)Ru(CO)_2]_2$ (**6**), by reaction of **1** with the alumina support, was observed. The identification of complex **6** was facilitated through its diagnostic ^1H NMR resonance of the unique Cp ring proton ($C_5Me_4\mathit{H}$), observed as singlet at $\delta = 4.46$ in [D$_6$]benzene. Formation of compound **6** from **1** during this workup procedure was later confirmed when pure complex **1** was subjected to column chromatography on alumina. The isolation of **1** was, however, accomplished by sublimation at 190 °C in high vacuum, after which compound **1** was obtained as an analytically pure, orange, air-stable solid in ca. 50% yield.

[a] Anorganisch-Chemisches Institut der Universität Zürich, Winterthurerstrasse 190, 8057 Zürich, Switzerland
E-mail: chburger@aci.unizh.ch

  1434−1948/01/0303−0795 $ 17.50+.50/0

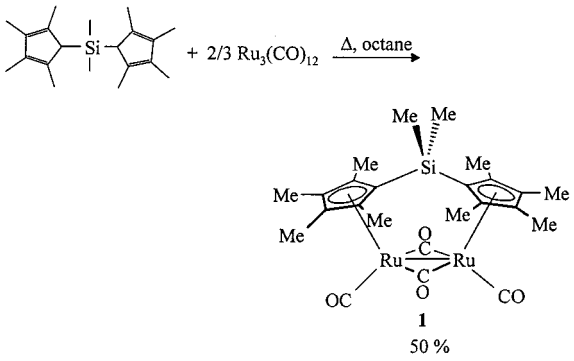

It should be noted at this point that in the X-ray crystal structure of the related parent complex $Me_2Si[(C_5H_4)Ru(CO)_2]_2$ (**2**), two bridging and two terminal CO groups were observed.[8] Differences in the solution and the IR spectra of **2** in KBr, however, suggested an equilibrium between the structure found in the solid state and another isomer, with four terminal CO groups, in solution. These results contrasted with the findings for the related methano-bridged diruthenium complex $CH_2[(C_5H_4)Ru(CO)_2]_2$ (**4**), for which four terminal CO groups were observed in the X-ray crystal structure, with just minor amounts of the corresponding bridged carbonyl complex $CH_2[(C_5H_4)Ru(\mu\text{-}CO)(CO)]_2$ in solution.[9]

The latter findings for the parent complex **2**, together with investigations by Angelici et al. into analogous CH_2- and C_2H_4-bridged complexes,[12] as well as a number of experimental and theoretical studies dedicated to the structural isomerism of CO ligands in the unbridged ruthenium and iron complexes $[CpFe,Ru(CO)_2]_2$, prompted us to look in detail at the solution structure of complex **1** and, in particular, consider the fluxional processes shown in Equation (2).[13–16] Before we address the solution behaviour of **1**, we will discuss the solid-state structure of compound **1** as observed in the single-crystal X-ray structure.

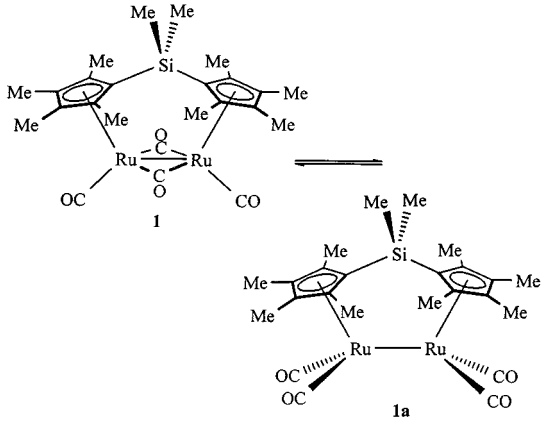

X-ray Crystal Structure of 1

The molecular structure of **1**, presented in Figure 1, illustrates that there are two types of carbonyl groups: i.e., two bridging and two terminal carbon monoxide ligands. This parallels findings from the X-ray crystal structure of the parent complex **2**. Details of data collection are summarized in Table 4; selected distances and angles are given in Table 1.

The molecule is located on a crystallographic C_2 axis passing through the Si atom and the midpoint of the Ru–Ru vector. A Ru–Ru single bond is indicated by a metal–metal distance of 2.7121(4) Å, with two symmetrical μ-bridging carbonyl groups [Ru1–C10 2.031(3), Ru1–C10A 2.032(3) Å] supporting the metal–metal bond. The metal–metal bond length is thus in the usual range observed for other cyclopentadienyl-bridged ruthenium complexes with μ-bridging carbonyl groups.[4,7,8,12] The remaining terminal CO groups [Ru1–C11 1.869(3) Å] are contained within the plane of the Ru metal centres and the centroids of the cyclopentadienyl rings. The ruthenium centres and the bridging carbonyl groups form a puckered four-membered ring, with a pucker angle of ca. 29°. A similar observation has been made for the ethano-bridged complex $C_2H_4[(C_5H_4)Ru(\mu\text{-}CO)(CO)]_2$ by Angelici et al.,[12] and has been rationalized on electronic grounds in a study by Hoffmann and co-workers.[16] From the top view of the molecular structure of complex **1** presented in Figure 1, it becomes immediately apparent that the molecular symmetry is close to idealized C_{2v} symmetry.

IR Data

In the IR spectrum of **1** in CH_2Cl_2 at room temperature, three absorptions in the ν(CO) range were detected: at 1980 (vs, terminal), 1940 (w, terminal), and 1757 (s, bridging) cm^{-1}. The band at 1757 cm^{-1} clearly demonstrates the presence of a μ-bridging carbonyl ligand consistent with the molecular structure of complex **1** observed in the solid state. Since we could detect just *two* terminal CO stretches in the terminal IR range, as would have been predicted for the μ-CO bridged complex **1**, there was initially no evidence for an additional isomer, such as the unbridged complex **1a**.

However, in the less polar solvent pentane, an additional *third* band could be observed in the terminal CO range [1992(vs), 1966(w), 1942(w)] in the IR spectrum. The presence of this additional vibration provided strong evidence for the presence of a further species, which was tentatively assigned as the isomer **1a**. In order to obtain further evidence for an exchange equilibrium between the bridging and presumed nonbridging complexes **1** and **1a**, we attempted variable temperature (VT) FT-IR measurements on **1** in pentane. Due to the quite low solubility of **1** in this solvent, however, these experiments proved to be difficult. While changes in the relative intensities of the absorptions consistent with a change in equilibrium concentrations were observed, no quantitative interpretation of the data was possible. We have therefore turned to VT NMR spectroscopic measurements on complex **1**; these are described in the following sections.

NMR Spectroscopic Analysis

The ^1H NMR spectrum of **1** in CD_2Cl_2 solution is temperature-*independent* (−95 °C to 35 °C) and displays three

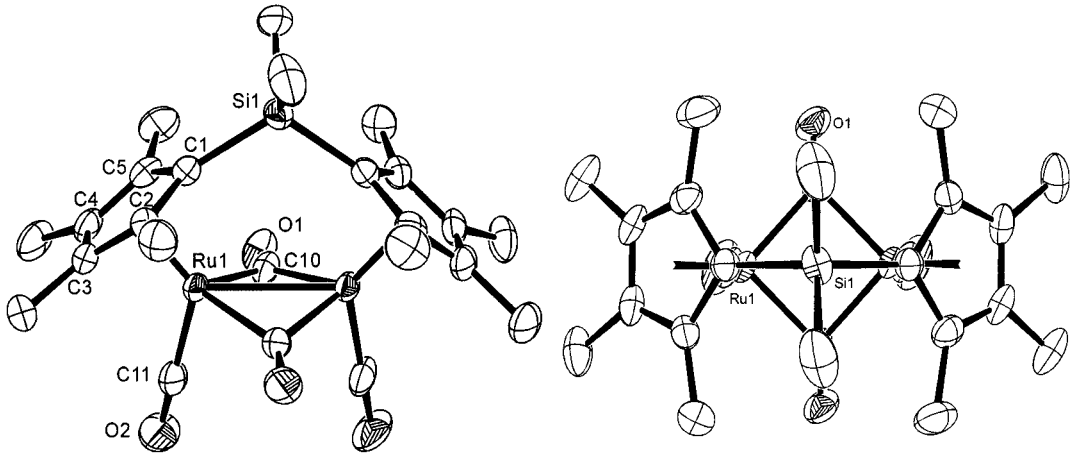

Figure 1. Ortep plots [side (left) and top (right)] of complex **1**; thermal ellipsoids are shown at the 50% probability level

Table 1. Selected distances [Å] and angles [°] with ESDs for complex **1**; Z1 is the midpoint of carbon atoms C1 to C5; "A" indicates symmetrically equivalent positions

Ru1−Ru1A	2.7121(4)	Ru1−C1	2.259(3)
Ru1−C2	2.283(3)	Ru1−C3	2.248(3)
Ru1−C4	2.248(3)	Ru1−C5	2.278(3)
Ru1−C10	2.031(3)	Ru1−C10A	2.032(3)
Ru1−C11	1.869(3)	C10−O1	1.180(4)
C11−O2	1.149(4)	Si1−C1	1.896(3)
$C-C(Cp)_{avg}$	1.44	Ru1−Z1	1.906
C10−Ru1−C10A	93.5(1)	C10−Ru1−C11	88.4(1)
C10−Ru1−Ru1A	48.7(1)	C11−Ru1−Ru1A	101.6(1)
Ru1−C10−Ru1A	83.2(1)	C1−Si1−C1A	110.7(1)
Ru1−C10−O1	136.6(2)	Ru1A−C10−O1	139.9(2)
Ru1−C11−O2	179.0(3)	C10−Ru1−Z1	121.5
C11−Ru1−Z1	130.1	Z1−Ru1−Ru1A	128.3
Z1−Ru1−Ru1A−Z1A	5.0	C11A−Ru1A−Ru1−Z1	182.7

sharp, well-resolved singlets for the ring methyl and dimethylsilyl groups, with a 2:2:1 integration ratio consistent with a C_{2v} symmetrical structure. In sharp contrast to this, we observed a strong temperature dependence for the ^{13}C NMR resonances of the CO ligands in **1**. At −95 °C, the 75.3 MHz ^{13}C NMR spectrum of **1** in CD_2Cl_2 solution displays two well-resolved resonances for two chemically inequivalent carbon monoxide ligands: at δ = 201.5 and 259.9, respectively. Upon warming, the ^{13}CO NMR resonances start to broaden at −85 °C and shift towards each other, until they completely disappear at −50 °C. For the Cp and dimethylsilyl groups, on the other hand, only sharp resonances with small temperature shifts were observed, which corresponds with the temperature independence of the ^1H NMR spectrum. Overall, the process was found to be completely reversible, which suggested an equilibrium between an *energetically preferred structure*, with two terminal and two bridging CO ligands (at lower temperature) as observed in the X-ray crystal structure, and an energetically *less favourable* complex with four terminal CO groups. This scenario is identical to the proposed exchange in the unsubstituted parent complex **2**.[8] In the fast-exchange regime, at higher temperatures, just one ^{13}C NMR CO resonance was therefore predicted in the time-averaged ^{13}C NMR spectrum. This was confirmed through ^{13}C NMR in $[D_{18}]$decahydronaphthalene at 100 °C and 50.3 MHz, with a single, sharp resonance at δ = 223.6 observed for the CO groups.

In order to provide unambiguous evidence for an equilibrium exchange between the terminal and bridging CO groups in complex **1**, through the intermediacy of isomer **1a** [Equation (2)], we resorted to 2D-^{13}C EXSY experiments. Thanks to the excellent solubility of **1** in CD_2Cl_2 even at low temperatures, this experiment appeared feasible for natural ^{13}C abundance in the CO ligands. From inspection of the line widths of the two chemically inequivalent ^{13}CO resonances at 75.3 MHz in the temperature range between −95 and −50 °C, a temperature of −65 °C was deemed a reasonable compromise between the line shape and exchange rate. The measurement was performed using a standard 2D EXSY pulse sequence over two days. The 2D EXSY spectrum is presented in Figure 2.

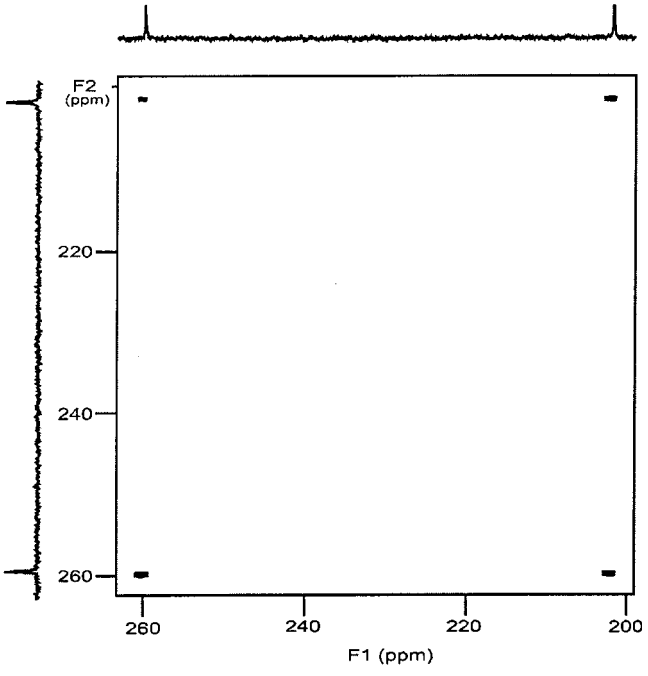

Figure 2. EXSY ^{13}C NMR spectrum (carbonyl range)

The substantial cross peaks between the two chemically inequivalent ^{13}CO resonances in the 2D EXSY spectrum provide excellent supporting evidence for the exchange of the bridging and terminal carbonyl groups, and clearly substantiate the exchange mechanism presented in Equation (2).

Subsequently, the determination of the activation parameters for the exchange process was attempted from a lineshape analysis of the temperature-dependent natural abundance ^{13}C NMR CO resonances. Unfortunately, this procedure turned out to be unreliable because of the strong dependence of the derived activation parameters on the natural line width in the slow-exchange regime, which could not be determined with sufficient accuracy. While the experimental and simulated ^{13}C NMR spectra were in excellent agreement, fits of the Eyring plot showed a large dependence on this parameter with derived $\Delta H^{\ddagger}$ values, varying by as much as 14 ± 4 kcal/mol. Further attempts to determine the rate of exchange by coalescence measurements were thwarted by difficulties in detecting the coalesced ^{13}C NMR carbonyl resonance, due to its extreme broadness. Further support for the observed exchange was therefore sought from DFT calculations, which are presented below. Prior to the discussion of these results, however, we will discuss a further reaction that was observed in the course of our investigations.

Photochemical Reaction of 1

In the course of studying photochemical CO ligand substitution reactions in **1**, we noticed the formation of a new compound in which the CO ligands had *not* been substituted. We hence studied the UV irradiation (medium pressure Hg lamp) of complex **1** by itself; i.e, in the absence of any added ligand [Equation (3)]. Conversion into the novel photochemical product **3** was also observed under these conditions and appeared to be clean (95% isolated yield) and fast. Essentially identical rates for the photochemical conversion were observed when a 1 M $NaNO_2$ solution as a UV/Vis cutoff filter (400 nm cutoff) was used in the photolysis experiments, implying that the lowest energy transition at 460 nm (broad band) in the UV/Vis spectrum of **1** in toluene is crucial to the photochemical process(es). The ^1H and ^{13}C NMR spectra of this product displayed five singlets (1:1:1:1:1 ^1H NMR integration ratio) for the methyl resonances of the Cp-methyl and the $SiMe_2$ groups and suggested a significant structural change compared to complex **1**. In the IR spectrum, the absence of bands in the expected range for μ-bridging CO groups was particularly noteworthy, and *four* bands for terminal CO groups at 2009 (vs), 1983 (vs), 1948 (vs), and 1922 (vs) cm^{-1} were observed in CH_2Cl_2 solution. The aforementioned spectroscopic data were consistent with the proposed structure for complex **3** shown in Equation (3), in which Si−C bond cleavage has occurred.

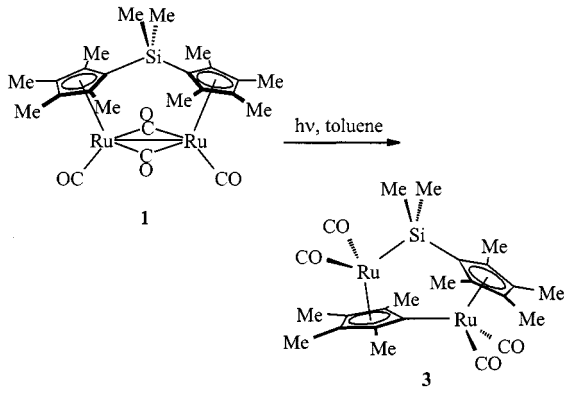

The structural assignment was unambiguously confirmed by the results of an X-ray crystal structure analysis (Figure 3). Details of data collection and selected distances and angles are summarized in Table 2 and 4.

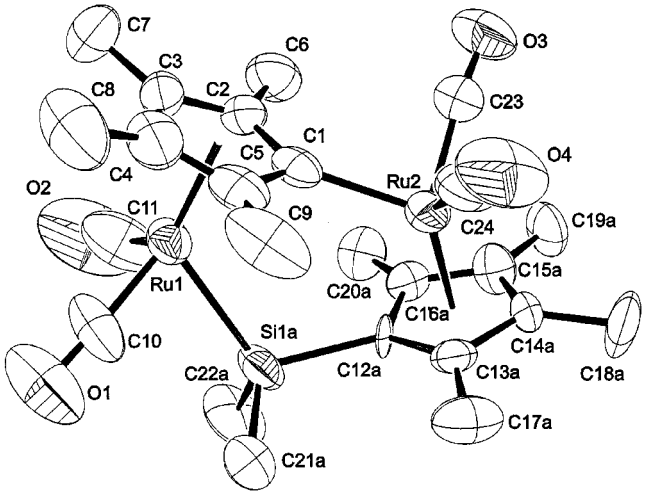

Figure 3. Ortep plot of the photochemical Si−C cleavage product, complex **3**; thermal ellipsoids are shown at the 50% probability level; only one of the disordered cyclopentadienyl rings (denoted by affix a) is shown

Since disordering of the $SiMe_2$ group and one of the attached Cp rings caused severe problems in the refinement, we will refrain from the discussion of bond angles and distances and instead briefly inspect the bond topology in complex **3**. In addition to the cleavage of the Si−C bond in the starting material, the Ru−Ru single bond observed in the starting material (complex **1**) is no longer present in the product, and new ruthenium−carbon and ruthenium−silicon bonds have been formed. There are four terminal carbonyl ligands, which explains the absence of bands in the μ-CO bridging ligand range in the IR spectrum.

Photochemical silicon-carbon cleavage in **1** parallels observations by Bitterwolf et al. in the unsubstituted parent complex **2**.[1] In the latter case, however, the reaction has been found to be more complicated, and competition between Si−C and, in addition, C−H activation of the cyclopentadienyl ring C−H group in the position *ortho* to the bridgehead atom was noticed. The apparent difference be-

Table 2. Selected bond lengths [Å] and angles [°] with ESDs for complex **3**; Z1 and Z2 are the midpoints of carbon atoms C1 to C5 and C12A,B to C16A,B, respectively; "A" and "B" indicate disordered positions

Ru1−Si1A,B$_{avg.}$	2.41(1)	Ru2−C1	2.146(11)
Ru1−C10	1.827(10)	Ru1−C11	1.820(13)
Ru2−C23	1.874(4)	Ru2−C24	1.838(11)
C10−O1	1.148(10)	C11−O2	1.189(13)
C23−O3	1.159(10)	C24−O4	1.176(12)
Ru1−Z1	1.91	Ru2−Z2$_{avg.}$	1.92
Ru1····Ru2	3.96		
C10−Ru11−C11	93.2(5)	C10−Ru−Si1A,B$_{avg.}$	87.8
C11−Ru1−Si1A,B$_{avg.}$	85.0	C10−Ru1−Z1	128.3
C11−Ru1−Z1	127.7	Si1A,B−Ru1−Z1$_{avg.}$	121.0
Ru1−C10−O1	176.6(11)	Ru1−C11−O2	175.7(12)
C23−Ru2−C24	90.7(5)	C1−Ru2−C23	90.4(4)
C1−Ru2−C24	90.8(4)	C23−Ru1−Z2$_{avg.}$	127.3
C24−Ru2−Z2$_{avg.}$	124.8	C1−Ru2−Z2$_{avg.}$	122.3
Ru2−C23−O3	174.3(8)	Ru2−C24−O4	176.2(11)
Z1−Ru1−C22−Si1−C12$_{avg.}$	−23	Z2−Ru2−C1−Ru1$_{avg.}$	0

tween the outcome of the photochemical reactions of complexes **1** and its unsubstituted congener **2** is best explained with a more difficult C−H activation step (higher activation barrier) at the sp^3-hybridized methyl group in **1**, as compared to the aromatic C−H group in **2**; there is ample evidence for this in the literature.[17,18] The higher barrier would thus lead to a preference for the Si−C activation step over its C−H counterpart. In an attempt to shed some light on the mechanism of this transformation, we have attempted to investigate this reaction thermally in a kinetic study. However, even under very harsh conditions (i.e. at temperatures of 180 °C and after an extended period of time), we could not detect thermal formation of the Si−C cleavage product **3**, and only unchanged starting material **1** was recovered, quantitatively. Prior to our DFT-calculations, which are detailed in the next section, we anticipated that complex **3** might not be obtained from **1** under thermal control, due to a thermally inaccessible barrier for the thermal transformation ($\Delta G^{\ddagger} > 40$ kcal/mol).

DFT Calculations

In view of the fact that complexes **1** and **3** might be interesting systems for light energy storage, we turned to DFT calculations to establish the thermodynamic preferences of this system. In addition, we wanted to assess the relative thermodynamic stabilities of the μ-CO bridged complex **1**, and its isomer **1a** with four terminal CO groups.

The molecular geometries found in the X-ray crystal structures of **1** and **3** were used as starting points for the geometry optimizations. A Becke−Perdew (BP86) functional[19,20] and TZVP basis-sets including a relativistic pseudopotential (Stuttgart−Dresden, ecp-28-mwb)[21] for the Ru centres and an SVP basis for the residual atoms were used at the initial stage in these calculations (basis I). After convergence of the optimizations at this level, TZVP-basis sets were applied for all atoms and the optimizations pursued further (basis II). Typically, this procedure required just a few optimization cycles to converge with the larger basis sets. An excellent agreement of the optimized geometries for complexes **1** and **3** with their X-ray crystal structures, with few deviations, was observed. As previously noticed in metal carbonyl complexes by others,[22,23] the unscaled calculated ν(CO) vibrational data were also in good agreement with the observed experimental IR data. The final calculated total energies are depicted graphically in Figure 4; selected calculated angles and ν(CO) vibrations of the optimized geometries, along with their experimentally determined values, are given in Table 3.

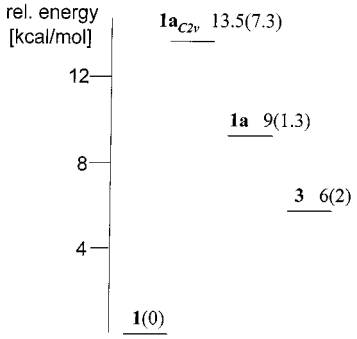

Figure 4. Relative energies of complexes **1**, **1a**, **1a$_{C2v}$**, and **3** as determined by DFT calculations using the BP86 functional; relative energies (kcal/mol) for B3LYP optimized geometries are included in parentheses (not on scale)

The results of the DFT calculations for complexes **1** and **1a** clearly provide supporting evidence for the higher thermodynamic stability of the μ-bridged carbonyl isomer **1**, with a preference of ca. 9 kcal/mol for **1**. However, on the basis of the fact that both isomers are present in comparable concentrations in pentane, as determined by IR spectroscopy, the theoretically predicted energy difference between the isomers **1** and **1a** is deemed to be too large. In view of this consideration, we have also included entropic contributions to this equilibrium; these are quite likely to be in favour of the unbridged isomer **1a**. This apparent unsatisfactory agreement may be attributed to solvation effects, which are not included in the (gas phase) calculations. It deserves special mention that strongly polar solvents were found to have a remarkable influence on the equilibrium position of such isomers.[13] However, since both isomers **1**

Table 3. Calculated and experimental distances, angles and ν(CO) vibrational data; DFT (BP-86) calculated vibrational data are unscaled and are given in cm^{-1}; Z denotes the centroid of a Cp ring; indexes b and t denote bridging and terminal; for essentially identical values, only averaged (avg.) data are given; rounded distances are given in [Å], angles in [°]; selected experimental data are included in parentheses

	Complex **1**	Complex **1a**	Complex $\mathbf{1a_{C2v}}$	Complex **3**
ν(CO)	1987w (1980)	2003 (s)		2008 (2009) (s)
ν(CO)	1955s (1940s)	1958 (w)		1990 (1983) (vs)
ν(CO)	1816s	1944 (s)		1953 (1948) (vs)
ν(CO)	1794s (1757s)	1932 (w)		1938 (1922) (vs)
d(Ru1−Ru2)	2.73(2.71)	2.87	2.97	
$d(Ru-Z)_{avg}$	1.96(1.91)	1.95	1.95	1.96 (1.92)
$d(Ru-CO_t)_{avg}$	1.86(1.87)	1.86	1.86	1.87 (1.84)
$d(Ru-CO_b)_{avg.}$	2.05(2.03)			
$d(Si-C_{Cp})$	1.92(1.90)	1.91	1.90	1.95
$d(Ru-\eta^1C_{Cp})$				2.13 (2.15)
d(Ru−Si)				2.44 (2.41)
Z−Ru1−Ru2	127.7(128.3)	120.7	123.6	
OC_t-Ru-Z	128.3(130.1)	127.0, 129.9	126.0	
$OC_t-Ru1-Ru2$	104.1(101.6)	85.7, 90.6	89.4	
$OC_t-Ru-CO_t$		90.4	91.6	90.0, 91.7
$OC_t-Ru-CO_b$	89.8(88.4)			
$OC_b-Ru-CO_b$	93.5(87.9)			
$Ru-C-O_b$	138.2(139.9)			
Si−Ru1−Z1				118.5
$Z2-Ru2-\eta^1C_{Cp}$				121.1
$OC_t-Ru2-\eta^1C_{Cp}$				91.2, 91.7
$OC_t-Ru1-Si$				86.9, 90.3
$OC_t-Ru1-CO_t$				91.7
$OC_t-Ru1-CO_t$				90.0
Z1−Ru1−Ru2−Z2	0.0	50.0	0.0_f	178.3
OC−Ru1−Ru2−CO		50.2, 140.6		

and **1a** are present even in the low-polarity solvent pentane, which can be quite confidently deemed compatible with the DFT calculations in the gas phase, it is suspected that the energetics of this system might not be appropriately represented by the applied BP86 functional. In addition, we have therefore performed calculations with the B3LYP hybrid functional,[24] which has been deemed to give excellent thermodynamic data not only for organic compounds but also for organometallic species. These calculations were performed with the large basis set (basis II) and the BP86-optimized geometries for the geometry optimizations. In general, the B3LYP-calculated relative energy differences (Figure 4) are appreciably smaller, while the energetic order of the isomers is unchanged. On the basis of the calculated difference of 1.3 kcal/mol between **1** and **1a**, a ca. 1:10 mixture in favour of the bridged isomer **1** would be predicted. Note that this is in good agreement with our temperature-dependent ^{13}C NMR and IR spectroscopic data.

It is worth mentioning that the geometry of the unbridged complex with four terminal CO groups (i.e. **1a**), converged at a structure that displays approximate C_2 symmetry, rather than C_{2v}. This can easily be seen from a plot along the metal-metal bond of **1a**, which is presented in Figure 5.

When the geometry optimizations were performed with C_{2v} symmetry constraints (complex $\mathbf{1a_{C2v}}$), the energy was found to lie 4.5 (BP86, 6 kcal/mol B3LYP) kcal/mol above that of **1a**. The presence of several imaginary frequencies in the range from −500 to $-64\ cm^{-1}$ nevertheless clearly showed that the optimized geometry for $\mathbf{1a_{C2v}}$ is not a stationary point (local minimum). Analysis of the latter frequencies showed that the major driving force behind the distortion to **1a** is due to the fact that it allows elongation of the $Si-C_{bridgehead}$ bond and shortening of the Ru−Ru bond. While we have no conclusive explanation for the energy differences between the two functionals, it should be noted that, in high level calculations on a nickel olefin system, an excellent agreement between these two functionals was observed, and also with calculations performed at the CASPT2 level.[25] It is noteworthy that we also observed negligible energy differences between B3LYP and BP86 functional in a related dicyclopentadienyl-bridged diruthenium system containing a CMe_2 rather than a dimethylsilyl

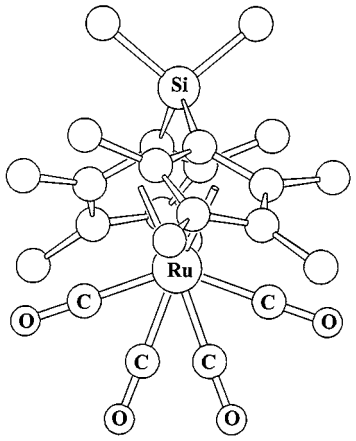

Figure 5. View along the metal−metal bond of the DFT-optimized structure of complex **1a**

bridge {i.e., $Me_2C[(C_5H_4)Ru(CO)_2]_2$}.[26] Furthermore, an inspection of the deviations between experimental and theoretical enthalpies for silicon-containing neutral compounds of the G2 test set[27] revealed large errors for both the BP86 (−7, +11 kcal/mol) and the B3LYP (−20, +3 kcal/mol) functionals, with the latter being more accurate for less-polar compounds. Hence, on the basis of these data, no clear judgement can be made as to either the appropriateness or the accuracy of these two widely applied functionals. Nevertheless, it is thought that despite the heavy usage of the B3LYP functional as the "ultima ratio" for DFT-derived energies in organometallic systems, some doubts seem appropriate and further calibration studies are definitely required.

Nevertheless, the most interesting result from the DFT calculations is the fact that the photochemically rearranged product **3** is estimated to be *6 kcal/mol less thermodynamically stable* (BP-86-functional, 2 kcal/mol for the B3LYP functional) than the metal-metal bonded starting material **1**. This view is further supported by single-point MP2 calculations (for details see Experimental Section) of the BP-86 optimized geometries **1** and **3**, which also showed a pronounced thermodynamic preference of 7 kcal/mol for complex **1** over **3**. For the unsubstituted parent complex $Me_2Si[(C_5H_4)Ru(CO)_2]_2$ (**2**), and its Si−C cleavage product **6** (the unsubstituted analogue of complex **3**), we calculate a similar thermodynamic situation, with compound **2** being energetically favoured by 6 kcal/mol (BP-86 functional, basis II). This sparked the idea that the photochemical transformation might be *reversed* thermally (**3** → **1**). We have therefore studied the thermolysis of **3** in toluene, which is described in the next section.

Thermolysis Experiments on Complex 3

The thermolysis experiments involving **3** were performed at temperatures up to 170 °C in sealed NMR tubes in [D_8]toluene and monitored by ^{1}H NMR spectroscopy. However, under these conditions thermal reconversion of complex **3** into **1** was *not* observed, even after extended reaction times (2 weeks) and at the highest possible temperatures. At present, it is therefore unclear whether large kinetic barriers account for the absence of a thermal reaction or whether the applied DFT methodology might not be accurate enough to make such predictions. However, it is especially noteworthy that we have observed an excellent agreement between experimentally determined (by DSC) energy differences and DFT calculations (within 1 kcal/mol) between constitutional isomers in the aforementioned, closely related C_1-bridged diruthenium system, $Me_2C[(C_5H_4)Ru_2(CO)_2]_2$.[26] At present, we therefore favour the notion that thermally unaccessible kinetic barriers (> 40 kcal/mol) prevent thermal reconversion of **3** to **1**.

Conclusion

The DFT calculations suggest that, in analogy to Vollhardt's fulvalenediyl diruthenium system,[5] rather inert, energetically disfavoured, photochemically rearranged products can also be obtained with other X-bridged (e.g., X = $SiMe_2$ here) dicyclopentadienyl systems. While the photochemical reaction could not be reversed for complexes **1** and **1a**, we will report on related functional systems in due course.

Experimental Section

The dimethylsilyl-bridged dicyclopentadiene ligand $Me_2Si(C_5Me_4H)_2$ was prepared according to published methods.[28] $Ru_3(CO)_{12}$ was used as received from Alfa. − ^{1}H NMR and ^{13}C NMR spectra were recorded on Varian Gemini 200 and 300 spectrometers operating at 200, 300 and 50.1, 75.4 MHz respectively. Chemical shifts are given in ppm and are referenced to the residual H solvent shift or ^{13}C NMR solvent shift. The assignment of ^{1}H NMR and ^{13}C NMR resonances is based on NOE and DEPT experiments. − IR spectra were measured on a Biorad-FTS 45 Fourier IR-spectrometer. − X-ray crystal structure analyses were performed on a STOE-IPDS image plate system with monochromated Mo-K_α (0.70713 Å) beam. − Elemental analysis were performed with a LECO CHNS-900 analyzer in our institute.

Synthesis of $SiMe_2[C_5Me_4Ru(CO)_2]_2$ (1): $SiMe_2(C_5Me_4H)_2$ (1 g, 3.33 mmol) and $Ru_3(CO)_{12}$ (1.4 g, 2.22 mmol) were refluxed for 5 days in 80 mL of *non-deoxygenated* octane. After this period, the resulting dark brown mixture was allowed to come to room temperature and the solvent removed in high vacuum. The solid residue was then sublimed at 190 °C and 10^{-2} Torr, with the product collected as an orange solid at the water-cooled sublimation finger, and finally recrystallized from CH_2Cl_2/ether at −30 °C. ***Caution:*** *The solid remainder of the sublimation is highly pyrophoric.* Yield: 1.04 g, 1.67 mmol, 50%. − ^{1}H NMR (25 °C, C_6D_6): δ = 1.93 (s, 12 H, $SiMe_2[\alpha$-$C_5Me_4]$), 1.80 (s, 12 H, $SiMe_2[\beta$-$C_5Me_4]$), 0.28 (s, 6 H, $SiMe_2[C_5Me_4]$). − ^{13}C{^{1}H} NMR (CD_2Cl_2, −65 °C): δ = 260.3(s, *C*O), 202.1 (s, *C*O) 110.6 (s, C_5Me_4), 103.8 (s, C_5Me_4), 78.9 (s, bridgehead C_5Me_4), 13.1 (s, C_5Me_4), 11.3 (s, C_5Me_4), 2.8 (s, $SiMe_2$). − $C_{10}D_{14}$, 100 °C: δ = 223.6 (s, *C*O), 110.1 (s, C_5Me_4), 105.1 (s, C_5Me_4), 79.1 (s, bridgehead C_5Me_4), 14.8 (s, C_5Me_4), 12.5 (s, C_5Me_4), 5.5 (s, $SiMe_2$). − IR (carbonyl range, CH_2Cl_2): $\tilde{\nu}$ = 1980(vs), 1940(w), 1757(s) cm^{-1}; IR (carbonyl range, KBr): $\tilde{\nu}$ = 1978(vs), 1934(w), 1768(s) cm^{-1}. − MS(EI, 70 eV): *m*/*z* (%) = 612 (100) [$M^{+\cdot}$], 584 (30) [$M^{+\cdot}$ − CO], 556 (100) [$M^{+\cdot}$ − 2 CO], 528 (100) [$M^{+\cdot}$ − 3 CO]. − $C_{24}H_{30}O_4Ru_2Si$ (612.7): calcd: C 47.05, H 4.94; found C 46.79, H 4.81.

Synthesis of Complex 3: Compound **1** (100 mg, 0.295 mmol) was dissolved in a Teflon-tap-sealed Pyrex Schlenk tube in 100 mL dry, thoroughly deoxygenated toluene, to give an orange solution. The Schlenk tube was immersed in a water bath kept at 10 °C and with the tube placed in close proximity to a medium pressure Hg lamp (HPK 125 W). An almost colourless (faintly yellowish) solution indicated the end of the photolysis reaction (usually 6 h). The solvent was removed in high vacuum and the product recrystallized from a toluene/pentane (1:1) mixture at −35 °C to give a colourless microcrystalline solid. Yield: 95 mg, 0.28 mmol, 95%. − ^{1}H NMR (25 °C, C_6D_6): δ = 2.14 (s, 6 H, C_5Me_4), 2.00 (s, 6 H, C_5Me_4), 1.88 (s, 46 H, C_5Me_4), 1.53 (s, 6 H, C_5Me_4), 0.78 (s, 6 H, $SiMe_2$). − ^{13}C{^{1}H} NMR (C_6D_6): δ = 205.9, 203.1 (*C*O), 129.4, 110.8, 105.3 104.7, 101.1, 76.4 ($Me_2SiC_5Me_4$, RuC_5Me_4), 16.4, 12.9, 11.9, 10.4, 8.3(s, C_5Me_4, $SiMe_2$). − MS (EI, 70 eV): *m*/*z* (%) = 612 (15) [$M^{+\cdot}$],

Table 4. Crystal and data collection parameters for compounds **1** and **3**

	1	**3**
Empirical formula	$C_{24}H_{30}O_4Ru_2Si$	$C_{24}H_{30}O_4Ru_2Si$
Formula mass	612.7	612.7
Habit	orange cube	colourless rect., parallelepiped
Crystal size [mm]	0.2 × 0.2 × 0.2	0.1 × 0.1 × 0.15
Crystal system	tetragonal	monoclinic
Space group	$P4_32_12$ (no. 96)	$P2_1/n$ (no. 14)
a [Å]	8.3800(3)	9.009(1)
b [Å]		16.551 (2)
c [Å]	32.1153(14)	16.963 (3)
β [°]		95.18 (2)
V [Å^3]	2508.5 (2)	2519.0(8)
Z	4	4
$\rho_{calcd.}$ [g/cm^3]	1.622	1.616
abs. coeff. [mm^{-1}]	1.28	1.28
F(000)	1232	1232
Temp [K]	183	183
abs. corr.	numerical	numerical
T_{min}, T_{max}	0.55, 0.99	0.30, 0.44
λ [Å], Mo-$K\alpha$	0.707173	0.707173
Scan type	Image Plate/-rotation	Image Plate/-rotation
2 Θ range [°]	4−52	4−52
No. of refl. meas. Total, unique	17008, 2429	18963, 4636
No. of parameters	141	280
$R_1(F^2 > 2\sigma(F^2))$	0.0198	0.0451
$wR_2(F^2 > 2\sigma(F^2))$	0.0540	0.0731
GooF, S	1.035	1.022
Res. el. dens. [e$^-$/Å^3]	0.30, −0.27	0.65, −1.1

584 (70) [$M^{+\cdot}$ − CO], 556 (100) [$M^{+\cdot}$ − 2 CO], 528 (80) [$M^{+\cdot}$ − 3 CO]. − IR (carbonyl range, CH_2Cl_2): $\tilde{\nu}$ = 2009(vs), 1983 (vs), 1948 (vs), 1922 (vs) cm^{-1}. − $C_{24}H_{30}O_4Ru_2Si$ (612.7): C 47.05, H 4.94; found C 46.67, H 4.68.

DFT and MP2 Calculations: The applied methodology is described in the text. The DFT calculations were performed with the Turbomole program suite[29] and using the RI-J-DFT (BP-86 functional) implementation (RIDFT) for the geometry optimizations and the calculation of the second derivatives.[30] Essentially identical energy differences were obtained with the BP-86 functional using the *pure* DFT rather than the RI-J-DFT method. The parallelized version of the Turbomole program package was used on our 12 CPU Linux cluster in all cases.[31] The single-point MP2 calculations on **1** and **3** were carried out using the geometry optimized with the BP-86 functional using the basis set described below. The RI implementation of MP2 available in Turbomole was used for these calculations (RIMP2),[32] with molecular orbitals possessing eigenvalues lower than −3 Hartrees treated as frozen core (MOs 1−35 for both **1** and **1a**). Final total energies in Hartree with unscaled zero-point energies in parentheses (in kJ/mol) for the optimized geometries using a Becke−Perdew (BP86) functional (RI-DFT method), TZVP basis sets[33] for all atoms and a Stuttgart−Dresden pseudopotential (ECP-28-mwb)[21] for the ruthenium centres are: **1**: −1713.84199(1232); **1a**: −1713.83043(1232); $\mathbf{1a_{C2v}}$: −1713.82021; **3**: −1713.83285(1236). Second derivatives were obtained numerically from finite differences. Using the same basis sets and ECPs, but the hybrid functional B3LYP instead, the following total energies were obtained for optimized geometries (cartesian gradients < 10^{-3} Hartree/Bohr): **1:** −1712.59622; **1a**: −1712.59412; $\mathbf{1a_{C2v}}$: −1712.58449; **3:** −1712.59309 [Hartree]. In the latter case, the BP86 optimized geometries were used as starting geometries. The MP2 total single point energies for compounds **1** and **3** with the HF energies and MP2 energy corrections in parentheses are: **1**: −1708.47894 [−1703.30867 (HF), −5.17028 (MP2)]; **3** −1708.46803 [−1703.33175 (HF), −5.13628 (MP2)]. The total energies in Hartrees for the optimized geometries (cartesian gradients < $2{\cdot}10^{-4}$ Hartree/Bohr) using the BP-86 functional with its RI-implementation in Turbomole, TZVP basis sets for all atoms and a Stuttgart−Dresden pseudopotential for Ru (ECP-28-mwb) of the unsubstituted parent complex **2** and the Si−C cleavage product **6** derived from it (the analogue of **3**), are: **2**: −1399.21427; **6**: −1399.20464.

X-ray Crystal Structure Analyses. − General Remarks: Suitable single crystals of complexes **1** and **3** were mounted on glass fibres in Paratone-N (oil) and were transferred on the goniometer head to the diffractometer and the crystal cooled to −80 °C in a N_2 cryostream. The data sets were collected with graphite monochromated Mo-K_α radiation (0.707173 Å) on a Stoe IPDS image plate diffractometer. Intensities were corrected for Lorentz and polarization effects and absorption corrections performed numerically with the faces and corresponding crystal dimensions determined using the STOE Faceit-Video CCD camera microscope system. The structures were solved using direct methods with the SHELXS-86 program package.[34] The refinements were carried out with SHELXL-93 using all unique F_o^2.[35] Except for complex **3**, all non-hydrogen atoms were refined anisotropically. The positions of the hydrogen atoms were calculated in idealized positions (C−H bonds fixed at 0.96 Å) and refined as a riding model with a fixed isotropic displacement factor of U = 0.08 Å^2. The details of the data collection and refinement, including R-values, are summarized in Table 4.

Complex 3: The cyclopentadienyl ring connected to the $SiMe_2$ unit and the dimethylsilyl group itself (atoms C12A,B−C22A,B, Si1A,B) were found to be disordered and were refined with two split positions (labelled A and B) and refined with occupation factors of 0.57 and 0.43. Carbon atoms C12−C22 were refined isotropically and all other non-hydrogen atoms anisotropically.

Crystallographic data for complexes **1** and **3** (excluding structure factors) have been deposited with the Cambridge Crystallographic Data Centre as supplementary publication numbers CCDC-140425 (**1**) and -140426 (**3**). Copies of the data can be obtained free of charge on application to CCDC, 12 Union Road, Cambridge CB2 1EZ, UK [Fax: (internat.) +44-1223/336-033; E-mail: deposit@ccdc.cam.ac.uk].

Acknowledgments

We are indebted to Professor Heinz Berke for his ongoing support.

[1] T. E. Bitterwolf, J. E. Shade, J. A. Hansen, A. L. Rheingold, *J. Organomet. Chem.* **1996**, *514*, 13−21.
[2] W. Xie, B. Wang, X. Dai, X. S., X. Zhou, *Organometallics* **1998**, *17*, 5406−5410.
[3] Y. Zhang, S. Xu, G. Tian, X. Zhou, J. Sun, *Organometallics* **1998**, *17*, 1122−1127.
[4] X. Zhou, Y. Zhang, W. Xie, S. Xu, J. Sun, *Organometallics* **1997**, *16*, 3474−3481.
[5] R. Boese, J. K. Cammack, A. J. Matzger, K. Pflug, W. B. Tolman, K. P. C. Vollhardt, T. W. Weidman, *J. Am. Chem. Soc.* **1997**, *119*, 6757−6773.
[6] C. Cremer, H. Jacobsen, P. Burger, *Chimia* **1997**, *51*, 650−653.
[7] T. E. Bitterwolf, M. B. Leonard, P. A. Horine, J. E. Shade, A. L. Rheingold, D. J. Staley, G. P. A. Yap, *J. Organomet. Chem.* **1996**, *512*, 11−20.
[8] X. Zhou, Y. Zhang, S. Xu, G. Tian, B. Wang, *Inorg. Chim. Acta* **1997**, *262*, 109−112.
[9] S. A. R. Knox, K. Macpherson, A. G. Orpen, M. C. Rendle, *J. Chem. Soc., Dalton Trans.* **1989**, 1807−1813.
[10] G. O. Nelson, *Organometallics* **1983**, *2*, 1474−1475.
[11] A. P. Humphries, S. A. R. Knox, *J. Chem. Soc., Dalton Trans.* **1975**, 1710−1714. O_2 has been recognized to accelerate the reductive elimination of H_2 in $CpRu(CO)_2H$. This fact is used in the improved synthesis of $[CpRu(CO)_2]_2$. N. M. Doherty, S. A. R. Knox, M. J. Morris, C. P. Casey, G. T. Whiteker, *Inorg. Synth.* **1990**, *28*, 189−191.
[12] C. Nataro, L. M. Thomas, R. J. Angelici, *Inorg. Chem.* **1997**, *36*, 6000−6008.
[13] J. G. Bullitt, F. A. Cotton, T. J. Marks, *Inorg. Chem.* **1972**, *11*, 671−676.
[14] F. A. Cotton, G. Yagupsky, *Inorg. Chem.* **1967**, *6*, 15−20.
[15] L. J. Farrugia and L. Mustoo, *Organometallics* **1992**, *11*, 2941−2944.
[16] E. D. Jemmis, A. R. Pinhas, R. Hoffmann, *J. Am. Chem. Soc.* **1980**, *102*, 2576−2585.
[17] A. E. Shilov, G. B. Shul′pin, *Chem. Rev.* **1997**, *97*, 2879−2932.
[18] C. L. Hill, *Activation and Functionalization of Alkanes*, John Wiley & Sons, Inc., New York, Chichester, Brisbane, Toronto, Singapore, **1989**.
[19] A. D. Becke, *Phys. Rev. A* **1988**, *38*, 3098−3100.
[20] J. P. Perdew, *Phys. Rev. B* **1986**, *33*, 8822−8824.
[21] D. Andrae, U. Häußermann, M. Dolg, H. Stoll, H. Preuß, *Theor. Chim. Acta* **1990**, *77*, 123−141.
[22] V. Jonas, W. Thiel, *J. Chem. Phys.* **1995**, *102*, 8474−8484.
[23] V. Jonas, W. Thiel, *J. Chem. Phys.* **1996**, *105*, 3636−3648.
[24] A. D. Becke, *J. Chem. Phys.* **1993**, *98*, 5648−5652.
[25] F. Bernardi, A. Bottoni, M. Calcinari, I. Rossi, M. Robb, *J. Phys. Chem. A* **1997**, *101*, 6310−6314.
[26] P. Burger, manuscript in preparation.
[27] L. A. Curtiss, K. Raghavachari, G. W. Trucks, J. A. Pople, *J. Chem. Phys.* **1991**, *94*, 7221−7230.
[28] C. M. Fendrick, L. D. Schertz, V. W. Day, T. J. Marks, *Organometallics* **1988**, *7*, 1828−1838.
[29] R. Ahlrichs, M. Bär, M. Häser, H. Horn, C. Kölmel, *Chem. Phys. Letters* **1989**, *162*, 165−169.
[30] K. Eichkorn, O. Treutler, H. Oehm, M. Häser, R.Ahlrichs, *Chem. Phys. Lett.* **1995** *242*, 652−660
[31] R. Ahlrichs, M. Bär, M. Häser, H. Horn, C. Kölmel, *Chem. Phys. Letters* **1989**, *162* 165−169. R. Ahlrichs, S. D. Elliott, U. Huniar, *Ber. Bunsen, Phys. Chem.* **1998**, *102*, 795−804; M. von Arnim R. Ahlrichs, *J. Comp. Chem.* **1998**, *19*, 1746−1757.
[32] F. Weigend, M. Häser, *Theor. Chem. Acc.* **1997**, *97*, 331−340; F. Weigend, M. Häser, H. Patzelt, R. Ahlrichs, *Chem. Phys. Lett.* **1998**, *294*, 143−152.
[33] H. Schäfer, H. Horn, R. Ahlrichs, *J. Chem. Phys.* **1992**, *97*, 2571−2577.
[34] G. M. SHELDRICK, *SHELXTL PLUS*, University of Göttingen, Germany, **1988**.
[35] G. M. Sheldrick, *SHELXL 93*, University of Göttingen, Germany, **1993**.

Received March 6, 2000
[I00086]